ChemElectroChem

Chemistry Europe
European Chemical Societies Publishing
ChemElectroChem

RESEARCH ARTICLE OPEN ACCESS

Relaxation of Electrochemically Induced Intermediate States Under Non-Operando Conditions

Wulyu Jiang[1,2] | Fei Tang[2] | Tian Liu[2] | Lu Xia[1] | Lin Gan[2]

[1]Faculty of Mechanical Engineering, RWTH Aachen University, Aachen, Germany | [2]Key Laboratory of Electrocatalytic Materials and Green Hydrogen Technology of Guangdong Higher Education Institutes and Shenzhen Key Laboratory of Advanced Layered Materials for Value-added Applications, Institute of Materials Research, Tsinghua Shenzhen International Graduate School, Tsinghua University, Shenzhen, Guangdong, P. R. China

Correspondence: Wulyu Jiang (wulv.jiang@rwth-aachen.de) | Lin Gan (lgan@sz.tsinghua.edu.cn)

Received: 9 January 2026 | **Revised:** 28 February 2026 | **Accepted:** 10 March 2026

Keywords: electrochemically induced intermediates | identical-location TEM | in situ Raman spectroscopy | oxygen evolution reaction | transition metal catalysts

ABSTRACT

Electrochemical polarization under oxygen evolution conditions often induces structural reconstruction from the parent phase in transition-metal-based catalysts, which are frequently interpreted as active intermediate species. Here, we investigate the relaxation behavior of electrochemically induced intermediates in spinel and hydroxide catalysts at controlled non-operando conditions by correlated spectroscopy and microscopy techniques. The oxyhydroxide phase formed at high anodic potentials remains stable after potential removal as long as electrochemical environments are maintained. In contrast, once the electrode is disconnected and the electrolyte is gradually removed, the intermediate state progressively relaxes back to the parent structure. Further drying treatments reveal that decreasing electrolyte activity markedly accelerates such structural recovery. These findings demonstrate that electrochemically induced intermediate structures should be regarded as boundary-condition-dependent states rather than intrinsically stable phases, highlighting the strong environment dependence of catalyst structural insights obtained under non-operando conditions.

1 | Introduction

Understanding the real working structure of electrocatalysts is essential for establishing reliable structure–performance relationships [1, 2]. Under anodic polarization in oxygen evolution reaction (OER), many transition-metal-based catalysts, e.g., typical spinel oxides, perovskites, and hydroxides, are reported to undergo pronounced surface reconstruction, giving rise to oxyhydroxide-like intermediate structures that are widely associated with enhanced catalytic activity [3–6]. Ideally, such well-defined states can be identified and tracked under in situ/operando conditions, where the catalyst is in its true electrochemical and interfacial environment. In practice, achieving simultaneous electrochemical fidelity and high-resolution structural characterization remains technically challenging [7]. For example, in situ electron microscopy under liquid environments often suffers from limited spatial resolution, restricted electrochemical windows, and beam-induced effects, while other in situ/operando spectroscopic techniques also face tradeoffs between temporal resolution, sensitivity, and environmental realism [8]. As a result, quasi-in situ and ex situ strategies, such as potential hold followed by rapid transfer, freezing, or drying prior to characterization, are frequently employed to probe electrochemically generated intermediate states [9–11].

The widespread use of such non-operando strategies implicitly assumes that the electrochemically induced intermediate state can be preserved after working conditions. However, while extensive efforts have been devoted to elucidating the reconstruction process from the parent phase to the transited structure under anodic polarization, the structural fate of the intermediate state once electrochemical boundary conditions are terminated has received far less attention. In particular, it remains

unclear whether these electrochemically induced intermediates can maintain, how rapidly they relax toward the parent phase, and which environmental factors govern this process for (ir)reversible surface reconstructions. Resolving these questions is essential for assessing the reliability of quasi-in situ and ex situ characterization and for distinguishing intrinsically stable catalytic phases from states that are stabilized only under specific electrochemical conditions.

In this work, we address this unresolved question by systematically examining the electrochemically induced intermediate states in transition-metal-based catalysts under controlled non-operando conditions. Using tailored electrochemical protocols combined with in situ Raman spectroscopy, we decouple the effects of electrochemical boundary conditions, including applied potential and electrolyte, on the structural evolutions of catalysts. By focusing on the behavior of the intermediate state beyond operando environments, this study aims to establish a clearer basis for interpreting quasi in situ and ex situ structural information of precatalysts, intermediates, and post-operando states.

2 | Results and Discussion

2.1 | Electrochemical Induced Structural Response of $NiFe_2O_4$ Spinel

Figure 1 first investigates the electrochemical activation behavior and the accompanying structural reconstruction of $NiFe_2O_4$ spinel catalyst under anodic conditions. The structure of pristine $NiFe_2O_4$ is confirmed by X-ray diffraction (XRD) (Figure 1a), which shows well-defined diffraction peaks characteristic of the spinel phase, indicating good structural ordering. The cyclic voltammogram (CV) curve (Figure 1b) displays distinct anodic and cathodic redox features prior to the onset of OER, which are commonly associated with Ni^{2+}/Ni^{3+} oxidation/reduction accompanying surface transition from parent spinel into oxyhydroxides [12, 13]. Such oxyhydroxide species are widely recognized as catalytically relevant structures for OER. Consistently, the emergence of OER current follows this redox transition, indicating that catalytic activity develops upon formation of the oxidized state. These redox responses indicate $NiFe_2O_4$ does not remain its precatalyst matrix, but forms a well-defined intermediate as the real working structure.

The corresponding in situ Raman spectra (Figure 1c) reveal pronounced changes in the vibrational fingerprints during the potential cycling. With increasing potential from open circuit voltage (OCV) to 1.5 V vs. RHE, characteristic spinel-related modes (A_{1g}: 680 cm^{-1}; T_{2g}: 480 cm^{-1}) disappear, while broadened spectral features emerge at 470 and 550 cm^{-1}, consistent with the formation of an electrochemically induced oxyhydroxide Ni(Fe)OOH phase [13–15]. Notably, the Raman fingerprints evolve reversibly with reductive potentials: the intermediate-state features recover to the spinel modes when stepping the potential back to 1.3 V vs. RHE. Such forward and reverse evolution between parent spinel and oxyhydroxide agrees well with the redox patterns in CV cycling, reflecting dynamic restructuring at surface. This reversible behavior likely arises from the structural compatibility between oxyhydroxide and spinel phases, where reduction facilitates reordering of the metal–oxygen framework and restoration of spinel coordination environments. As a result, the catalytically relevant intermediate states at OER are not permanently robust, but sensitive to electrochemical environments.

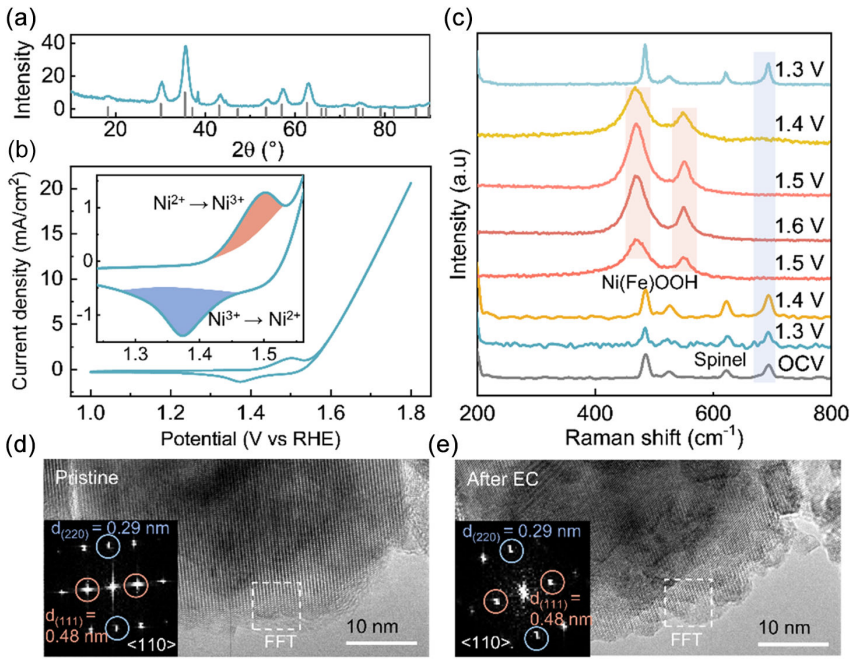

FIGURE 1 | Electrochemical activation and structural evolution of $NiFe_2O_4$ under anodic conditions. (a) XRD pattern of pristine $NiFe_2O_4$ catalyst. (b) CV curve recorded in 0.1 M KOH, with the inset of anodic and cathodic redox features. (c) In situ Raman spectra collected at different electrochemical states, showing the emergence and evolution of electrochemically induced intermediate features (highlighted in red) upon anodic polarization, together with the attenuation of characteristic spinel-related modes (highlighted in blue). (d,e) ILTEM images before (pristine) and after electrochemical operation (holding at 1.5 V for 30 min), respectively. The insets are corresponding fast FFT patterns at representative regions.

This reversible spectroscopic behavior is complemented by identical-location TEM (IL-TEM) analysis performed on the same particle before and after OER process (Figure 1d,e). High-resolution TEM images show that the particle retains well-defined lattice fringes characteristic of spinel, with fast Fourier transform (FFT) patterns from representative regions remaining indexed to spinel phase (both feature typical lattice spacings of 0.48 and 0.29 nm attributed to (111) and (220) planes of spinel along the <110> zone axis). Although modest changes in surface roughness and local crystal domain orientation are observed due to structural reconstruction during electrocatalysis, including reduced lattice fringe continuity and smaller crystal size in certain regions, the preserved characteristic lattice spacings confirm the retention and recovery of spinel structural ordering in the After EC sample.

Together, the intermediate oxyhydroxide from spinel is a reversible, metastable surface configuration that exists only under specific electrochemical conditions, whereas non-operando structural probes such as IL-TEM predominantly reveal the resting spinel phase. This distinction underscores the necessity of operando/in situ characterization for identifying such electrochemically induced states, and cautions against directly equating non-operando structural observations with the true working-state structures.

2.2 | Structural Evolution of Oxyhydroxides Under Non-Operando Conditions

Following the above in situ identification of an electrochemically induced intermediate state by Raman, ex situ ILTEM only captures the parent spinel structure. This observation raises a key question: is the apparent disappearance of the intermediate state intrinsic to potential or electrolyte under electrochemical environments?

To figure it out, the applied anodic potential was first removed while maintaining electrical connection to OCV (1.46–1.47 V vs. RHE initially, 1.35–1.40 V vs. RHE after 30 min). Under these conditions, the time-resolved Raman spectra (Figure 2a) show that the spectral features of oxyhydroxide induced after holding at 1.7 V vs. RHE persist over extended durations for 30 min. Despite the absence of an external driving potential, no immediate recovery to the spinel fingerprint is observed, indicating that the intermediate state does not spontaneously relax under OCV conditions as long as electrochemical environments are preserved.

In contrast, a distinct structural evolution is observed when both the applied potential and the liquid conditions are gradually removed (Figure 2b). Upon electrical disconnection and out of electrolyte (Air dry 0 min), the intermediate-state NiFeOOH features are intense. After 5 min, visible electrolyte dried as observed by coupled microscopy in Raman spectrometer, and then, the following Raman spectra (Air dry 5–15 min) track progressive attenuation of oxyhydroxide signals, accompanied by the re-emergence and enhancement of spinel characteristics. These behaviors imply the intermediate state under OER is not intrinsically stable outside the electrochemical environment and relaxes toward the parent spinel structure once electrochemical constraints are lifted. This structural relaxation corresponds to the loss of the active species associated with OER. Accordingly, the electrochemical environment governs not only the formation but also the persistence of this metastable structure configuration, thereby controlling and influencing the observed catalytic activity and long-term structural stability.

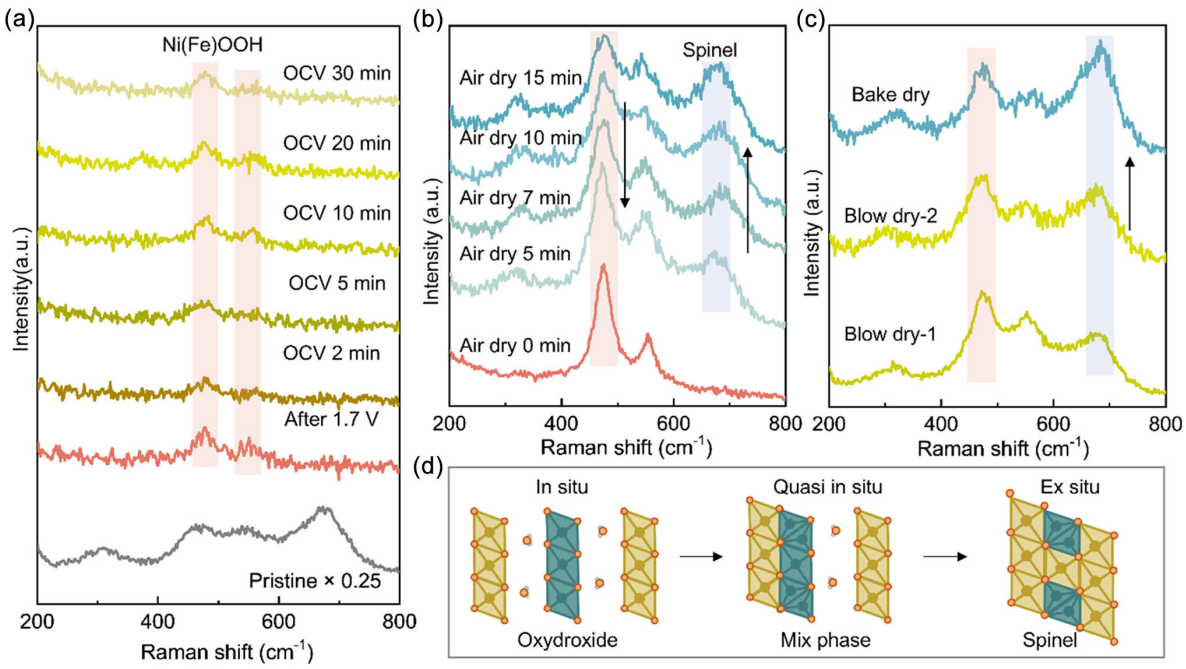

FIGURE 2 | Evolution of electrochemically induced intermediate states from $NiFe_2O_4$ under controlled non-operando conditions. (a) Time-resolved Raman spectra collected after removal of the anodic potential while maintaining electrical connection. (b) Raman spectra after air-drying with removal of both the applied potential and liquid environment. (c) Representative Raman spectra after blow-dry (2 min) and bake-dry (60°C in the oven for 2 min) conditions. (d) Schematic illustration of the evolution of surface structural states under different electrochemical boundary conditions.

Such structural relaxation process was deliberately controlled under postoperation environments in Figure 2c. After blow-dry and bake-dry for 2 min, the intermediate-state Raman bands diminish more rapidly, accompanied by a faster recovery of the spinel fingerprint. The Raman signal of spinel after baking catalysts (Bake dry) dominates compared with blow-dry samples at two different regions (Blow dry-1 and Blow dry-2) probably due to the complete drying of electrolytes at elevated temperatures. While such phase transition is kinetically dependent on post-treatment, the overall spectral evolution pathway remains consistent with the relaxation identified after electrical disconnection. This accelerated behavior confirms that the disappearance of the electrochemically induced intermediate state is a reproducible relaxation rather than a time-dependent measurement artifact, and its kinetics can be modulated by postoperation environmental conditions.

Collectively, the evolution of surface structural states under different electrochemical boundary conditions shows that the postoperation follows the same pathway but proceeds at different kinetics. As summarized in Figure 2d, when electrochemical boundary conditions are preserved (in situ), the electrochemically induced intermediate state remains stabilized even after potential removal. In contrast, quasi in situ or ex situ conditions, which inherently involve the release of electrochemical circuit and three-phase interfacial constraints, lead to structural relaxation toward the parent spinel phase.

2.3 | Validation of Condition-Dependent Intermediate: Evidence From $Co(OH)_2$

Such boundary-condition-dependent behavior identified for $NiFe_2O_4$ spinel was further validated in another layered hydroxide system. In situ Raman spectra of initial $Co(OH)_2$ (Figure 3a) show the emergence of oxyhydroxide vibrational features consistent with the formation of a CoOOH-like active state under OER-relevant anodic polarization [16, 17]. Notably, upon removal of the applied potential to OCV, these features remain largely unchanged for 50 min, indicating that the electrochemically induced active state is preserved as long as electrochemical boundary conditions are maintained. This behavior closely mirrors the persistence of Ni(Fe)OOH features observed in Figure 2a under OCV with electrical connection.

The postoperation evolution of this active state is further resolved in Figure 3b by selectively modulating the surrounding environments. After drying the electrode, the Raman spectra return to the parent $Co(OH)_2$ fingerprint (Dried), indicating relaxation of the oxyhydroxide state back to the hydroxide phase. Subsequent OER polarization reactivates the active-state features (OER-R), confirming the reversibility of the structural transformation. Importantly, when electrical disconnection is introduced while retaining the electrolyte (No EC), the active-state Raman features persist for at least 30 min. In contrast, removal of the electrolyte (No KOH), even with electrical connection maintained, leads to a rapid re-emergence of $Co(OH)_2$ modes, which progressively dominate the spectra (No KOH-15 min). To distinguish the role of electrolyte composition (OH^- ions or H_2O), the alkaline electrolyte was replaced with DI water at the surface of CoOOH after OER activation of $Co(OH)_2$ (Figure 3c). Under these water-contact conditions, the characteristic CoOOH Raman features remain stable for 60 min despite the absence of alkaline electrolyte and applied potential. Only upon removal of water and subsequent drying does the spectrum gradually revert to the $Co(OH)_2$. These results confirm that stabilization of the oxyhydroxides is governed primarily by the liquid-phase interfacial environment rather than by alkaline electrolyte composition.

These observations demonstrate that oxyhydroxides represent metastable surface phases whose stability is governed by electrochemical equilibrium with the electrolyte rather than by the

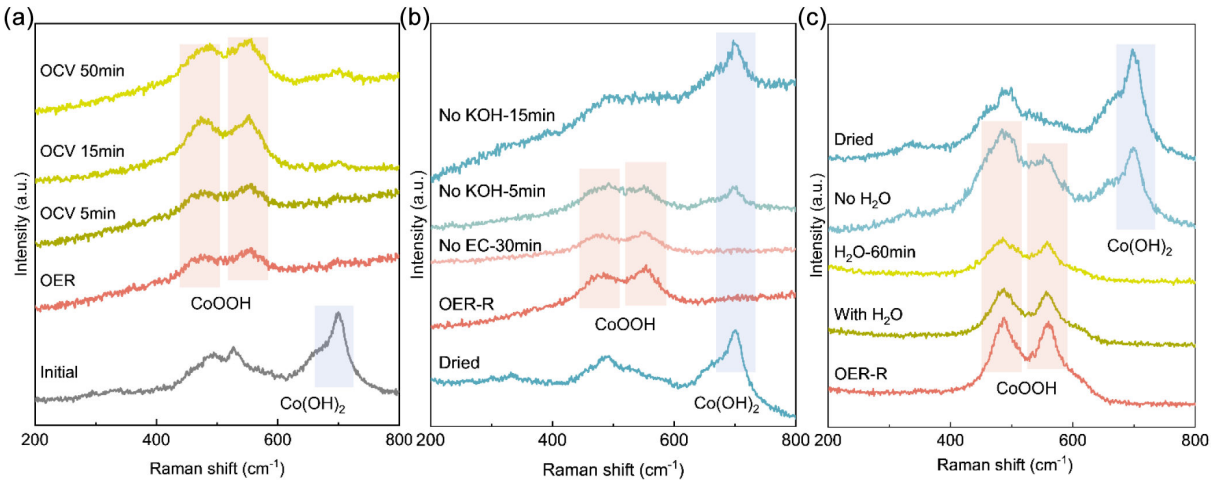

FIGURE 3 | Environment-dependent evolutions of electrochemically induced active states in $Co(OH)_2$. (a) Raman spectra of $Co(OH)_2$ during initial activation under first OER-relevant anodic polarization, followed by monitoring under OCV conditions for 50 min after removal of the applied potential. (b) Controlled postoperation Raman measurements to decouple the roles of electrical connectivity and electrolyte presence. The electrode was first dried to back to the parent $Co(OH)_2$ phase, then reactivated to CoOOH under anodic polarization. Subsequently, the electrical connection was removed while retaining the alkaline electrolyte for 30 min (No EC), followed by removal of the electrolyte while maintaining the electrical connection (No KOH). (c) Controlled liquid environment to probe the influence of electrolytes. After electrochemical activation to CoOOH in 1 M KOH, the electrolyte was replaced by rinsing with DI water, and Raman spectra were collected under water-contact conditions for 60 min, and further drying process to evaluate the structural stability of CoOOH in the absence of alkaline electrolyte.

applied potential alone. Formation of the oxyhydroxide involves coupled proton–electron transfer that shifts the metal–oxygen framework into an oxidized configuration stabilized by interfacial equilibrium with ionic and electronic chemical potentials in the electrolyte. As long as the electrode remains immersed, the electrolyte enables dynamic charge compensation and proton exchange, which stabilizes the oxidized coordination environment and lowers the effective free energy of the oxyhydroxide phase relative to its dry-state counterpart. Interfacial hydration further screens local charge imbalance and reduces lattice strain associated with higher oxidation states, thereby kinetically hindering structural relaxation [18, 19]. In contrast, removal of the electrolyte disrupts this electrochemical equilibrium by eliminating ionic compensation, proton exchange pathways, and solvation stabilization, shifting the system toward a bulk thermodynamic regime in which the oxyhydroxide phase is no longer energetically favored. Consequently, the lattice relaxes toward the thermodynamically stable bulk structures, namely hydroxide in the Co system and spinel in the NiFe system, driven by redistribution of metal oxidation states and minimization of lattice free energy.

These mechanistic insights highlight that postreaction handling is an integral part of structural characterization, and establish a practical basis for quasi-in situ characterization to ensure accurate representation of operando-relevant catalyst structures. The observed persistence of the oxyhydroxide structure under electrolyte-supported conditions provides a finite time window during which the electrochemically stabilized state can be captured without applied bias. For characterization techniques that are compatible with the liquid-contained samples, such as XRD, Raman, or X-ray absorption spectroscopy, maintaining electrolyte contact during transfer and measurement is recommended, even after electrical disconnection, to preserve the electrochemically stabilized environment. For techniques that require removal of any liquid, such as electron microscopy, electrolyte withdrawal should be performed immediately prior to measurement and with minimal delay, to capture the transient structural state before disruption of electrochemical equilibrium induces structural relaxation.

3 | Conclusion

In this work, we elucidate the boundary-condition-dependent nature of electrochemically induced transient intermediates in OER catalysts using in situ Raman spectroscopy combined with controlled electrochemical protocols. Across both a spinel oxide ($NiFe_2O_4$) and a layered hydroxide ($Co(OH)_2$), anodic polarization induces active-state structures that are readily observed under in situ conditions but relax toward their parent phases once electrochemical boundary environments are gradually released. While these active states can persist after potential removal under specific postoperation constraints, the reversible evolution is governed by how electrochemical connectivity and electrolyte presence are terminated.

Overall, this study clarifies a critical but often overlooked aspect of electrocatalyst characterization: the structural state probed after operation is dictated not only by the applied potentials, but also by the overall electrochemical environmental boundary. These findings provide a clear recognition for interpreting quasi-in situ and ex situ measurements and underscore the importance of explicitly defining postoperation protocols when correlating structure with catalytic performance in non-operando catalysis.

4 | Experimental Section

4.1 | Chemicals and Materials

$NiFe_2O_4$ and $Co(OH)_2$ catalysts were synthesized based on previously reported methods. For $NiFe_2O_4$ nanoparticles: thermal decomposition of $Ni(acac)_2$ and $Fe(acac)_3$ in benzyl ether using oleic acid and oleylamine as surfactants, followed by sequential heating at 200°C and 265°C [12]. For $Co(OH)_2$ nanoplates: $Co(NO_3)_2{\cdot}6H_2O$ (12.5 mmol) was dissolved in deionized water (40 mL) under stirring. NaOH pellets (1 g) were then added to the solution, and the mixture was stirred at 1200 rpm for 10 min to form a precipitate [20]. The resulting $Co(OH)_2$ was collected and washed thoroughly with deionized water and ethanol.

4.2 | Electrochemical Characterization

Electrochemical OER measurements were performed on a BioLogic SP-150 workstation using a standard three-electrode configuration with a rotating disk electrode (Pine Research). A glassy carbon (GC) electrode served as the working electrode, with a Pt wire counter electrode and a Hg/HgO reference electrode. The catalyst ink was prepared using Nafion (5 wt%, Sigma–Aldrich) as the ionomer binder and drop-cast onto the GC electrode with a catalyst loading of 0.08 mg/cm^2. Electrochemical measurements were conducted in 1 M KOH for $Co(OH)_2$ and 0.1 M KOH for $NiFe_2O_4$ catalysts respectively. CV measurements were carried out between 1.0 and 1.7 V vs. RHE (iR corrected) at a scan rate of 100 mV/s. All other electrochemical preparation parameters and testing protocols, including activity and stability evaluations, were performed following established procedures reported previously [21, 22].

4.3 | Raman Spectroscopy

In situ Raman measurements were carried out using a previously reported electrochemical Raman setup [12]. Quasi in situ or ex situ Raman spectra were collected under control electrochemical conditions or drying conditions, as specified below:

1. OCV conditions: the applied anodic potential was terminated and the potentiostat was switched to OCV mode while the working, counter, and reference electrodes remained immersed in the electrolyte and electrically connected, allowing the electrode potential to evolve freely without external bias.
2. Air-dried condition: the electrode was removed from the electrolyte and exposed to ambient lab air (approximately 20°C–25°C, relative humidity 30%–50%) without forced convection for natural drying.
3. Blow-dried condition: the electrode was removed from the electrolyte and dried under a gentle nitrogen gas flow at room temperature for 2 min to accelerate liquid evaporation while minimizing thermal effects.

4. Bake-dried condition: the electrode was removed from the electrolyte and dried in the oven at a controlled temperature (60°C) for 2 min, ensuring complete removal of residual electrolyte and adsorbed water.

5. Electrolyte removal with maintained electrical contact condition: after switching to OCV mode, the electrolyte was gradually withdrawn from the electrochemical cell using a pipette while maintaining electrical connection between all electrodes and the potentiostat. This procedure preserved the electrical circuit while progressively eliminating electrolyte–electrode ionic contact.

6. Electrolyte-retained without electrical connection condition: the electrode remained immersed in the electrolyte after termination of the applied potential, and all electrical connections to the potentiostat were disconnected, allowing the electrode to relax in the electrolyte without external electrical control.

A 532-nm or 633-nm laser was used as the excitation source. Each spectrum was averaged over multiple acquisitions to improve the signal-to-noise ratio.

4.4 | ILTEM

IL-TEM was performed using a customized electrochemical TEM holder configuration, following previously reported procedures [11, 23]. A 200-mesh Au TEM grid coated with a holey carbon support film was mounted onto a glassy carbon electrode and used directly as the working electrode during electrochemical measurements.

Conflicts of Interest

The authors declare no conflicts of interest.

Data Availability Statement

The data that support the findings of this study are available from the corresponding author upon reasonable request.

References

1. J. Huang, A. H. Clark, N. Hales, et al., "Oxidation of Interfacial Cobalt Controls the pH Dependence of the Oxygen Evolution Reaction," *Nature Chemistry* 17 (2025): 856.

2. L. Xia, B. F. Gomes, W. Jiang, et al., "Operando-Informed Precatalyst Programming towards Reliable High-Current-Density Electrolysis," *Nature Materials* 24 (2025): 753.

3. Y. Duan, S. Sun, Y. Sun, et al., "Mastering Surface Reconstruction of Metastable Spinel Oxides for Better Water Oxidation," *Advanced Materials* 31 (2019): 1807898.

4. Y. Sun, J. Wang, S. Xi, et al., "Navigating Surface Reconstruction of Spinel Oxides for Electrochemical Water Oxidation,," *Nature Communications* 14 (2023): 2467.

5. A. Bergmann, E. Martinez-Moreno, D. Teschner, et al., "Reversible Amorphization and the Catalytically Active State of Crystalline Co_3O_4 during Oxygen Evolution," *Nature Communications* 6 (2015): 8625.

6. E. Fabbri, M. Nachtegaal, T. Binninger, et al., "Dynamic Surface Self-Reconstruction Is the Key of Highly Active Perovskite Nano-Electrocatalysts for Water Splitting" *Nature Materials* 16 (2017): 925.

7. A. Prajapati, C. Hahn, I. M. Weidinger, et al., "Best Practices for In-Situ and Operando Techniques Within Electrocatalytic Systems," *Nature Communications* 16 (2025): 2593.

8. F. M. Alcorn, P. K. Jain, and R. M. van der Veen, "Time-Resolved Transmission Electron Microscopy for Nanoscale Chemical Dynamics," *Nature Reviews Chemistry* 7 (2023): 256.

9. J. Xu, L. Chang, Y. Wei, et al., "Size-Dependent Core–Shell Fine Structures and Oxygen Evolution Activity of Electrochemical IrO_x Nanoparticles Revealed by Cryogenic Electron Microscopy," *ACS Nano* 18 (2024): 29140.

10. M. Arenz and A. Zana, "Fuel Cell Catalyst Degradation: Identical Location Electron Microscopy and Related Methods," *Nano Energy* 29 (2016): 299.

11. W. Jiang, F. Tang, and L. Gan, "Electrochemical Stability of Au-TEM Grid with Carbon Supporting Film in Acid and Alkaline Electrolytes for Identical-Location TEM Study," *Journal of Electroanalytical Chemistry* 826 (2018): 46.

12. F. Tang, T. Liu, W. Jiang, and L. Gan, "Windowless Thin Layer Electrochemical Raman Spectroscopy of Ni-Fe Oxide Electrocatalysts during Oxygen Evolution Reaction," *Journal of Electroanalytical Chemistry* 871 (2020): 114282.

13. W. Jiang, A. Y. Faid, B. F. Gomes, et al., "Composition-Dependent Morphology, Structure, and Catalytical Performance of Nickel–Iron Layered Double Hydroxide as Highly-Efficient and Stable Anode Catalyst in Anion Exchange Membrane Water Electrolysis," *Advanced Functional Materials* 32 (2022): 2203520.

14. J. Wei, Y. Shao, J. Xu, et al., "Sequential Oxygen Evolution and Decoupled Water Splitting via Electrochemical Redox Reaction of Nickel Hydroxides," *Nature Communications* 15 (2024): 9012.

15. H. Qian, J. Wei, C. Yu, et al., "In Situ Quantification of the Active Sites, Turnover Frequency, and Stability of Ni–Fe (Oxy)hydroxides for the Oxygen Evolution Reaction," *ACS Catalysis* 12 (2022): 14280–14289.

16. C. Jing, T. Yuan, L. Li, et al., "Electrocatalyst with Dynamic Formation of the Dual-Active Site from the Dual Pathway Observed by In Situ Raman Spectroscopy," *ACS Catalysis* 16 (2022): 10276–10284.

17. H. Zhong, Q. Zhang, J. Yu, et al., "Fundamental Understanding of Structural Reconstruction Behaviors in Oxygen Evolution Reaction Electrocatalysts," *Advanced Energy Materials* 13 (2023): 2301391.

18. J. Gallenberger, H. Moreno Fernández, A. Alkemper, et al., "Stability and Decomposition Pathways of the NiOOH OER Active Phase of NiO_x Electrocatalysts at Open Circuit Potential Traced by Ex Situ and In Situ Spectroscopies," *Catalysis Science & Technology* 13 (2023): 4693.

19. H. Moreno Fernández, A. Alkemper, et al., "Kinetic Analysis of the Self-Discharge of the NiOOH OER Active Phase in KOH Electrolyte: Insights from in-situ Raman and UV–Vis Reflectance Spectroscopies," *Journal of Catalysis* 440 (2024): 115823.

20. W. Jiang, L. Xia, B. Ferreira Gomes, et al., "Facile and Green Synthesis of Well-Defined Nanocrystal Oxygen Evolution Catalysts by Rational Crystallization Regulation," *Small* 20, no. 21 (2024): 2308594.

21. W. Jiang, W. Lehnert, M. Carmo, and M. Shviro, "Effects of Electrochemical Parameters on the Evaluation of Nickel-Based OER Catalysts under Alkaline RDE Conditions," *ACS Electrochemistry* 1 (2025): 2787–2799.

22. W. Jiang, W. Lehnert, and M. Shviro, "The Influence of Loadings and Substrates on the Performance of Nickel-Based Catalysts for the Oxygen Evolution Reaction," *ChemElectroChem* 10 (2023): e202200991.

23. R. M. Aran-Ais, Y. Yu, R. Hovden, et al., "Identical Location Transmission Electron Microscopy Imaging of Site-Selective Pt Nanocatalysts: Electrochemical Activation and Surface Disordering," *Journal of the American Chemical Society* 137 (2015): 14992.